John Mbũrũ Ngũgĩ, Sandra Richter, Marina Braun-Unkhoff, Clemens Naumann, Uwe Riedel, A study on fundamental combustion properties of, oxymethylene ether-1, the primary reference fuel 90, and their blend: Experiments and modeling, Combustion and Flame (2022) 111996.

The original publication is available at www.elsevier.com

http://dx.doi.org/10.1016/j.combustflame.2022.111996

A study on fundamental combustion properties of oxymethylene ether-1, the primary reference fuel 90, and their blend: Experiments and modeling

John Mbũrũ Ngũgĩ[a]*, Sandra Richter[a], Marina Braun-Unkhoff[a], Clemens Naumann[a] and Uwe Riedel[b]

[a] Institute of Combustion Technology, German Aerospace Center (DLR), 70569 Stuttgart, Germany

[b] Institute of Low-Carbon Industrial Processes, German Aerospace Center (DLR), 03046 Cottbus, Germany

*Corresponding author: John Mbũrũ Ngũgĩ
German Aerospace Center, Pfaffenwaldring 38-40, 70569 Stuttgart, Germany
phone: +49 711 6862 8864
Email: john.mburu@dlr.de

Dedicated to the special issue for Katharina Kohse-Höinghaus

Abstract

Oxymethylene ethers (OME_n) are discussed as attractive carbon-reduced alternative fuels because they offer the potential to inhibit the formation of soot particles. In the present study, the effect of oxymethylene ether-1 (OME_1) addition to a gasoline surrogate, here the primary reference fuel 90 (PRF90), on ignition delay times and laminar burning velocities was investigated. Ignition delay times of OME_1, PRF90, and their blend with OME_1 blending fraction of 70% (by liquid vol.) were measured in a shock tube over a wide range of conditions: fuel-air ratio $\varphi = 1.0$, dilution of 1:5 with N_2, $T = 950$ K-2000 K, and initial pressures of 1, 4, and 16 bar. Laminar burning velocities of OME_1, PRF90, and their blend with OME_1 blending fraction of 30% (w/w) were measured by using the cone angle method at a preheat temperature of 473 K, φ = 0.6-2.0, and at pressures of 1, 3, and 6 bar. The experimental data sets have been compared to predictions made using the in-house DLR reaction mechanism, which was developed for surrogate modeling of gasoline, diesel, and jet fuels as well as oxygenated species such as alcohols (C_1-C_4) and oxymethylene ether (OME_n, n = 1-5). The results revealed that the DLR mechanism satisfactorily predicts the experimental data for ignition delay times and laminar burning velocities of both the individual fuels and the blend. Both the experimental and calculation results show that ignition delay times of OME_1 / PRF90 are shorter than those of PRF90 for 1, 4, and 16 bar. The values of the measured burning velocities also agree with the predicted corresponding laminar flame speed data, except at high pressure (6 bar) and at high φ values. The effects of increasing OME_1 fraction in the blend was tested, with the results showing a corresponding non-linear decrease of ignition delay times. Sensitivity analyses and radical mole fractions analysis calculations were performed to interpret the effect of adding OME_1 to PRF90 on ignition delay times and laminar flame speeds.

[Keywords: Oxymethylene ether, gasoline surrogate, ignition delay time, laminar burning velocity, blending , shock tube, reaction mechanism]

1 Introduction

The transport sector, due to its heavy dependence on fossil fuels, is a major contributor of CO_2, which is the most prominent greenhouse gas (GHG) connected to climate change [1-3]. Furthermore, tail-pipe emissions of soot and particulate matter (PM) are an issue due to strict emission regulations [4, 5]. Therefore, it is widely accepted that a wide range of approaches is needed to promote low-emission mobility in terms of carbon and air pollutants, such as the use of electric batteries, hydrogen, and the use of carbon-neutral fuels (biofuels and synthetic fuels) [6-8]. Currently, due to technological challenges such as energy storage, performance of batteries, and the requirement for new infrastructure for energy distribution in the case of *e.g.*, hydrogen, the use of alternative fuels like alcohols, ethers, and renewable synthetic fuels as additives or substitutes offer a promising solution within the already existing infrastructure and ability to run in engines with no modification [9-11].

Oxymethylene ethers (OME_n) are carbon-reduced synthetic fuels that can act as a drop-in replacement of conventional fuels because they have good soot-reduction potential and good auto-ignition characteristics [12-15]. The general formula of oxymethylene ethers is CH_3-O-$(CH_2O)_n$-CH_3, with $n \geq 1$. They can be produced renewably via gasification of biomass or by using the power-to-liquid technology (PtL) based on the catalytic conversion of green hydrogen and carbon dioxide [9, 14]. Green hydrogen is produced by electrolysis of water by use of renewable electricity, *i.e.* from wind power, while CO_2 can be captured directly from air or from industrial processes; for instance, during steel or cement production [9, 16].

In recent years, the use of oxymethylene ethers (OME_{1-5}) in diesel engines in neat form and as fuel additive has been studied by many researchers. The results demonstrated a remarkable decrease in soot and CO in the exhaust due to their high oxygen content and the absence of C-C bonds in their fuel structure [12]. To promote further the application of OME_n in engines, a detailed knowledge on their fundamental combustion properties, *i.e.* ignition delay times and laminar burning velocities, is a pre-requisite, also, for the development and optimization of their chemical kinetic reaction models. The combustion kinetics of the smallest oxymethylene ether (OME_1) has been widely studied in terms of chemical kinetic modeling and combustion experiments, *i.e.,* in shock tubes, burners, flow reactors, jet-stirred reactors, and rapid-compression machine (RCM), and have been previously reviewed in several studies: for example, by Cai *et al.* [16], Ngugi *et al.* [17], and Herzler *et al.* [18]. Besides the research work on individual oxymethylene ethers (OME_n), detailed knowledge on fundamental combustion properties of blends of OME_n and surrogate mixtures for gasoline and diesel can provide useful references for their engine application. It is well understood that blending of gasoline with high cetane boosters such as ethers among others has opened up the use of gasoline in compression ignition engines, *i.e.*, HCCI operation mode offering improved combustion and emission characteristics [19-21]. Up to now, studies on the fundamental combustion kinetics of blends of OME_n and surrogate mixtures for gasoline are very scarce in the literature. The few studies available on this subject address the

combustion of OME_1 with *n*-heptane as a gasoline surrogate [22-24]. Gao *et al.* [22] studied the oxidation of OME_1 / *n*-heptane mixtures using the atmospheric pressure jet-stirred reactor in the temperature range between 500 - 1100 K, φ = 0.5 - 2.0, and at a residence time of 2.0 s. They also developed a chemical kinetic model for describing low-temperature oxidation of OME_1 / *n*-heptane blends. Goeb *et al*. [23] studied the ignition process and soot formation of OME_1 and its blend with *n*-dodecane as diesel surrogate fuel using a high-pressure spray chamber. The experimental data obtained was used to validate their chemical kinetic mechanism for oxidation of OME_1 / *n*-dodecane blends. Hu *et al*. [24] studied the ignition delay times of OME_1 and its blends with *n*-heptane as a primary reference fuel for gasoline and diesel using the shock tube method at pressures of 2 and 10 atm, φ = 0.5, 1.0 and 2.0, and T = 1100 –1600 K. The results showed that the addition of OME_1 decreased ignition delay times of n-heptane. They also built and validated a new chemical kinetic model for oxidation of OME_1 / n-heptane blends. Ren *et al.* [25] and Lin *et al*. [26] developed compact chemical kinetic mechanisms to describe combustion of OME_3 / PRF90 blends in internal combustion engines. The mechanisms were validated with homogeneous charge compression ignition (HCCI) data for the blend and literature data for ignition delay times, laminar flame speeds, and species concentration profiles of individual OME_3 and PRF90.

The main objective of this work is to enlarge the knowledge on combustion of blends of OME_1 with surrogate mixtures for gasoline by presenting new experimental data for ignition delay times and laminar burning velocities. Because of the composition complexity and the extensive variability of petroleum-derived gasolines, surrogate modeling for gasoline is notably challenging [27, 28]. Binary mixtures of iso-octane and *n*-heptane, referred as "primary reference fuels" (PRFs), are widely used to mimic gasoline with a focus on research octane number (RON) and motor octane number (MON), and thus reflect the target gasoline's ignition tendencies and heat release [28-30]. Ternary mixtures of *iso*-octane, *n*-heptane, and toluene have been suggested for enhanced reproducibility of the octane sensitivity S (S = RON - MON) [31, 32]. The primary reference fuel 90 (PRF90), a binary compound of 90% *iso*-octane (iC_8H_{18}) and 10% *n*-heptane (nC_7H_{16}) by liquid volume, was chosen to represent the gasoline surrogate in this work since it has been demonstrated to be a viable gasoline surrogate fuel [33, 34]. However, in terms of ignition and heat release, more accurate multi-component surrogate combinations are necessary to replicate gasoline fuels at low NTC temperatures [27]. Researchers can employ multi-component surrogate formulations to capture additional target gasoline attributes such as carbon / hydrogen ratio, distillation curve, carbon types, and many more, which are required to better understand and model the complexity underlying chemistry of gasoline combustion [27]. In the present work, new experimental data for oxidation of OME_1 / PRF90 blend are reported: (i) Ignition delay times of a blend of 70% OME_1 and 30% PRF90 by liquid volume are obtained by the application of the shock tube method for φ =1.0, dilution ratio of 1:5 in N_2, and at initial pressures of 1, 4, and 16 bar; and (ii) Laminar burning velocities of a blend of 30% OME_1 + 70% PRF90 (% v/v) were obtained at pressures of 1, 3, and 6 bar by using a Bunsen burner and applying the cone angle method. The results achieved are compared to those obtained

at similar conditions for: (i) PRF90 / synthetic air within the present work, and for (ii) OME_1 / synthetic air as reported in our previous work [17]. These experimentally obtained data sets are compared to modeling predictions using the in-house model DLR mechanism [35]. Furthermore, the results of OME_1 and PRF90 are compared to predictions using the literature models of Cai *et al.*[16] and Mehl *et al.*[36], respectively. The ability of the DLR mechanism to predict the ignition delay times and laminar burning velocities of the pure fuel components and binary mixtures is tested. The results obtained in this work will help to overcome challenges observed in chemical kinetic modeling of fuel blends not seen when only testing pure fuels.

2 Experimental investigation

In this section, the experimental approach which covers the shock tube method of ignition delay times measurement and the cone angle method of laminar burning velocities measurement is presented.

2.1 Ignition delay time measurements

2.1.1 Experimental set-up

All the ignition delay time measurements in this work were carried out in the shock tube (ST) facility at the DLR's Institute of Combustion Technology, Stuttgart. The schematic diagram of this shock tube is presented in Fig. 1. The shock tube has an inner diameter of 9.82 cm, a driver section of 5.88 m, and a driven section of 11.35 m. The shock tube is operated in double-diaphragm configuration introducing a small intermediate section between the driver and driven sections. To achieve the tailored interface condition and thus, to extend the observation period, helium and argon mixtures, both with purity of above 99.996%, were used as the components of the driver gas. The flow of driver gas components was controlled by Bronkhorst (model E-7100-RAA) mass flow controllers. The driven section was heated at a constant temperature of 353 K to prevent the condensation of the fuel. Before each experiment, the entire tube is evacuated to pressures below 5.0×10^{-6} mbar by a turbomolecular pump. More detailed description of the shock tube facility and of the procedure is given in the literature; see [37-41].

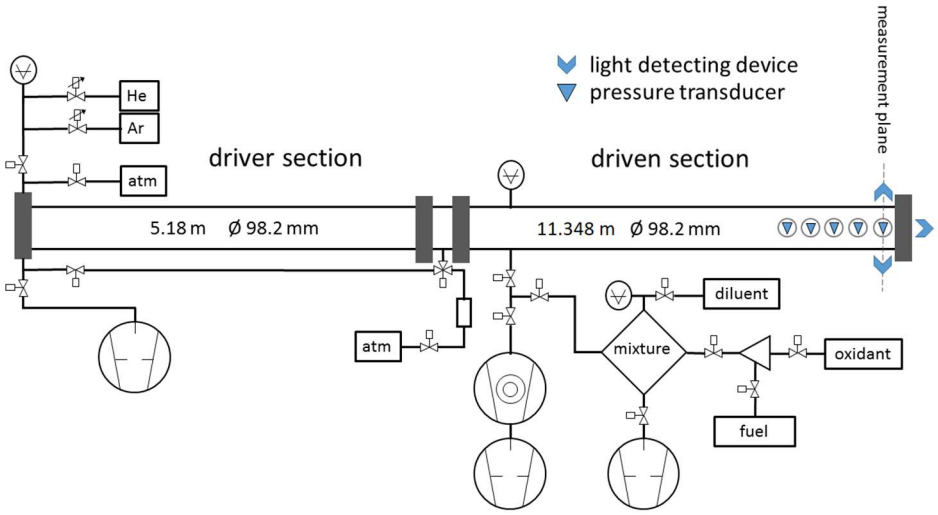

Figure 1: Schematic illustration of the shock tube used in the present work [41]. The measurement plane is located 10 mm from the end flange.

The diagnostic section of the shock tube is located 10 mm away from the end-plate and has four equally spaced fast-response pressure transducers (type PCB 113B24) flush-mounted on the side wall (see Fig. 1). They trigger the time-interval counters (type HAMEG HM 8123) to record the time for the arrival of the incident and reflected shock wave at each pressure transducer. The velocity of the incident (u_1) and the reflected shock waves (u_5) is then calculated from the recorded time intervals and the constant distance of 200 mm between the pressure transducers. The speed of the incident shock wave at the end plate is derived by linear extrapolation of the axial velocity profile in the x-t diagram to the end-plate. The conditions behind the reflected shock wave, *i.e.* temperature (T_5) and pressure (p_5), are calculated from the one-dimensional normal shock equations with measured incident shock velocity (u_1), initial temperature (T_1), pressure (p_1), fuel / oxidizer / diluent composition, and thermodynamic properties as the input parameters. For the shock tube, the initial temperature behind shock waves has been investigated by CO-absorption / emission measurements in CO / argon mixtures and was found to correspond to the initial temperature as calculated by the Rankine-Hugoniot equations providing the incident shock velocity within ±1.5% @ 1000K [42]. In addition, the relative error in the measured incident shock wave velocity for this shock tube is less than 1% which translates to an uncertainty of about ±10K in initial temperature and ±1.8 % in initial pressure behind the reflected shock wave. For this shock tube, the observation period is limited to about 3 ms when using helium as the only component of the driver gas because the decompression wave generated following the Mach number change of the reflected shock wave after passing the contact surface. The observation period is extended by avoiding the decompression wave and ensuring that the reflected shock wave continues to propagate almost unattenuated after passing the contact surface by tailoring, *i.e.* by adapting the impedance of the driver gas to match that of the test gas by adding argon to helium.

2.1.2 Mixture preparation

The stoichiometric mixtures of OME_1 / synthetic air, PRF90 / synthetic air, and 70% OME_1 + 30% PRF90 / synthetic air mixtures at a dilution ratio of 1:5 with nitrogen (20% fuel-oxidizer mixture: 80% N_2) were prepared in a 128 L stainless-steel heated mixing vessel, which was evacuated to pressures below 5 * 10^{-6} mbar by a turbomolecular pump. The temperatures of the mixing vessel and the shock tube were adapted to the minimum temperature required to keep the fuel in the combustible mixtures in gaseous form, *i.e.*, 313 K for OME_1 and 353 K for PRF90 and the blend. We use gas chromatography to test the quality of the mixture and thus, to ensure the fuel in the combustible mixture is in gaseous form. Due to the high level of dilution (about 95% N_2) applied, these temperatures were determined to be sufficient. Prior to preparing the combustible mixture, the vessel is isolated from the shock tube, flushed with N_2, and evacuated to low pressures of approximately 10^{-5} mbar. The combustible mixture was prepared monometrically by injecting separately the fuel, synthetic air, and N_2, in this order to their respective partial pressures into the evacuated vessel. The mixture was used after 24 hours to ensure a good mixing. Synthetic air, O_2, and N_2 were obtained from Linde with a purity of 99.999%. OME_1 was obtained from Sigma-Aldrich with a purity of 99.0%, and *iso*-octane and *n*-heptane were both obtained from Merck each with a purity of 99.00 %. The detailed composition of the combustible mixtures studied is provided in Table 1. For combustible mixtures with the blended fuels, *i.e*. PRF90 and OME_1 / PRF90 blend, the blended fuel mixtures were prepared in advance in a small glass container. The combustible mixtures with these fuels were then prepared via direct injection into the mixing vessel as previously described.

Table 1: Composition of the combustible mixtures (φ = 1.0 and dilution level of 1:5 with nitrogen) for ignition delay time measurements

Mixture	Composition / ppm
OME_1 / synthetic air / N_2	9490 OME_1 38277 O_2 952233 N_2
PRF90 / synthetic air / N_2	2872 iC_8H_{18} 319 nC_7H_{16} 39308 O_2 957901 N_2
70% OME_1 + 30% PRF90 / synthetic air / N_2	1612 iC_8H_{18} 179 nC_7H_{16} 4179 OME_1 38489 O_2 955541 N_2

PRF90: 90% *iso*-octane (iC_8H_{18}) + 10% *n*-heptane (nC_7H_{16}) by liquid volume; synthetic air: 20% O_2 + 80% N_2; Dilution ratio of 1:5 means 20% fuel - air mixture + 80% N_2 by molar fractions.

2.1.3 Determination of ignition delay times

In this work, all ignition delay times (IDTs) are based on chemiluminescence emissions of the excited CH* species measured at 431 nm. The CH* emission was observed at the measurement plane (radial)

as well as through the end-plate window (axial) by a narrow-band pass filter (Hugo Anders, FWHM = 10 nm) and detected by Hamamatsu R3896 photomultipliers. The emission signal from the photomultipliers is then amplified by FEMTO HLVA-100 logarithmic amplifiers. In addition, ignition is also monitored at the measurement plane by measuring the pressure profile with a fast-response pressure transducer (Kistler 603B) (see Fig. 1) which is protected against flash temperature by a thin layer of RTV116 silicon rubber. A Savitzky–Golay filter with a polynomial of third degree is used to smooth the pressure signal in a moving window of 5 points, with 40 iterations. All the ignition delay time values in this work were derived by measuring the time interval between the instance of arrival of the incident shock wave at the end plate ($t = 0$) and the time of occurrence of the maximum emission of the excited CH* species measured at the side port (radially) and through the end plate window (or alternately) as shown in Fig. 2.

Figure 2 shows an example plot of a pressure and normalized CH* emission signal (axial and radial) obtained from a single experiment for 70%OME_1 + 30%PRF90 / synthetic air with an initial temperature of 958 K and initial pressure p_i = 15 bar behind the reflected shock wave. In the first stage, the pressure is observed to increase in two steps that respectively correspond to the passage of the incident and the reflected shock wave. After the reflected shock wave has passed, the pressure increases gradually in a non-linear way and reaches a maximum at about 5800 µs due to viscous gas dynamics, *i.e.* due to dampening of the reflected shock wave due to its interaction with the boundary layer left behind by the incident shock wave. From here, the pressure remains constant (see dashed line in Fig. 2) and then gradually rises from about 7100 µs after the reflected shock wave has passed the contact surface due to the combined effect of over-tailoring and influence of heat release. Once the tailored condition is achieved, then the pressure should remain uniform even after the reflected shock wave passes the contact surface until the mixture ignites or is decompressed by the reflected head rarefaction wave.

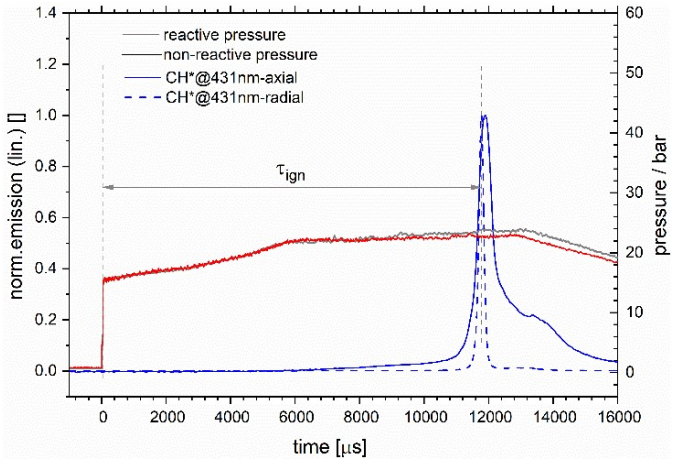

Figure 2: Example of a pressure and normalized CH* emission signals (axial and radial) obtained for an OME_1 + PRF90 (70:30) / synthetic air mixture at φ = 1.0, p_i = 15 bar, T_{init} = 958 K, and a dilution of 1:5 with N_2.

To account for the facility-dependent rise in pressure due to gas dynamics when calculating ignition delay times, a normalized experimentally derived pressure profile $p(t) / p(t/s=0)$ is provided to the calculations. The characteristic pressure profile $p(t)$ is derived from experiments without ignition (or from those with long ignition delay times) and with non-combustible mixtures with almost similar acoustic impedance. For fuels with early heat release, like OME_1 in this case, the pressure profile is considered up to the point of distortion due to heat release. In this case, the pressure profiles from non-combustible mixtures with similar acoustic impedance provide the check for heat release in reactive experiments. By considering the normalized pressure profiles from selected experiments, the pressure profile is derived applying a non-linear fit. Because this pressure profiles does not show any distortions due to heat release, the fit is extrapolated at a constant level after maximum compression is reached, which is connected to the contact surface transition of the reflected shock front. Behind this point, the pressure should remain constant in a well-tailored case until the decompression due to the rarefaction wave arrives at the end wall; see non-reactive pressure trace in Fig. 2.

Due to the distance between end wall and radial observation port(s) and the different speeds of the combustion wave and the reflected shock wave, the radially derived ignition delay times are related to the measurements at the end wall through a blast wave correction procedure using deflagration velocity obtained from the highest temperature measurements in the series [43, 44]. This approach assumes that ignition always starts at the end wall, where the high temperature and high-pressure conditions are triggered by the reflected shock wave, and that emission must first propagate with the combustion wave before it can be detected via the radial measuring port. At our experimental conditions, correction due to blast wave is up to 20 µs. The significance of the error (on side wall data) due to blast wave correction reduces as temperature reduces. In our measurements, the level of dilution applied (1:5 with N_2) also reduces the blast wave speed, and thus, increases the discrepancy between the radial and axial data. Nevertheless, for extremely short ignition delay times, generally around and below 10 µs, the axially derived ignition delay time can be taken as an upper bound because the blast wave correction is not required for axial emission detection. The detection setup comparison of both emission signals (radial with axial) decreases the inaccuracy of blast wave correction at the maximum temperatures to ±30%, despite the blast wave correction process being required for the radial port emission detection measurements [41]. Additionally, the experimental error on side-wall ignition delay timings attributed to the spatial resolution of the side wall CH* detection system is estimated to be 12 µs @ 500 m/s blast wave velocity. Although restricted by slits, light from a 6 mm diameter zone in the center of the tube reaches the detector of the photomultiplier via the optics of the side wall detection system. The time it takes the combustion wave (blast wave) to pass through this region is related to the spatial resolution, and it is denoted as the uncertainty of the side-wall ignition delay times.

2.2 Measurement of laminar burning velocities

Laminar burning velocities (S_u) of OME_1, PRF90, and their blend with 30% OME_1 (w/w) were measured using a Bunsen burner and applying the cone angle method. The measurements were carried out at a preheat temperature of 473 K, equivalence ratios φ between 0.6 to 1.8, and for pressures of 1, 3 and 6 bar. The experimental approach has been described in detail in previous publications [38, 45]; thus, only a brief description is given here.

The preparation of fuel-O_2-N_2 mixture is carried out first: The different fuels / fuel mixtures were vaporized at a temperature which depends on the (final) boiling point of the fuel at the chosen pressure and mixed with preheated nitrogen (Linde, purity 99.99%). This mixture is homogenized and adjusted to the preheat temperature of 473 K. Oxygen (Linde, 99.95%) is added in the second homogenization step. The flow rates of nitrogen and oxygen were controlled by calibrated Bronkhorst (type F-111B) mass flow controllers; their ratio was set to mimic air (79:21 = N_2:O_2). The time of contact with O_2 at preheat temperature in the fuel preparation line is limited to less than 0.5 s at 1 bar and 5 s at 6 bar, respectively. The flow rate of the fuel is controlled by a HPLC-pump (type LC-20AD, Shimadzu). OME_1 was obtained from Sigma-Aldrich with a purity of 99.0%. The combustible mixture was burnt at the outlet of a converging nozzle. The conical shaped flames were stabilized over a wide range of fuel-air ratio φ by the use of a co-flow: air at fuel-rich conditions ($\varphi \geq 1$) and a mixture of 5% CH_4 + 5% H_2 + 90% N_2 for fuel lean flames ($\varphi \leq 1.0$), as reported in our previous work [45]. The laminar burning velocity S_u is derived from the cone angle method according to Eq. (1), where the cone angle α is derived from the images of the conical shaped flames captured by a CCD-camera (type Imager Intense, LaVision) and the velocity v_u of the unburned gas is determined from the measurement.

$$S_u = v_u \cdot \sin\alpha \qquad (1)$$

A comprehensive experimental uncertainty for the determination of the burning velocities was carried out. The results showed that the uncertainties depend predominantly on pressure and fuel-air ratio. At 1 bar, the uncertainty is determined to be in the range of ± 2% to ± 5%, with about ± 6% for very fuel rich mixtures ($\varphi \geq 1.9$) and up to ± 9% for very fuel lean mixture ($\varphi < 0.8$). At elevated pressures, the uncertainties are between ± 2% and ± 9%, with up to ± 13% for fuel rich mixtures ($\varphi > 1.4$). These uncertainties are mainly due to difficulties in stabilization of the flames resulting to varying cone angles. Further influences on uncertainties are due to pressure fluctuations and the accuracies of the mass flow controllers.

2.3 Simulations

All measurements in this work are compared to the modeling predictions using the in-house DLR mechanism [35]. The DLR mechanism is a high-temperature semi-detailed reaction mechanism designed for surrogate modelling of a wide range of hydrocarbon fuels, *i.e.* jet fuels, gasoline, and diesel surrogates, and it has been extended to include reactions of oxygenated species such as alcohols (C_1-C_4)

and oxymethylene ethers (OME_n, n = 0-5) [35]. To the best of our knowledge, the DLR mechanism is the only complete mechanism that can describe the combustion of blends of OME_{1-5} with surrogate mixtures for gasoline and diesel in a common combustion environment. Furthermore, the measurements of OME_1 are compared against calculations made with the Cai *et al.*[16] model. The measured data for PRF90 are compared to model calculations using the most recent version of the Lawrence Livermore National Laboratory (LLNL) gasoline surrogate by Cheng *et al.*[27] and the older version by Mehl *et al.*[36]. Table 2 shows the specifics of the reaction mechanisms. The LLNL mechanisms [27, 36] were expanded with a sub-model of OH* and CH* chemiluminescence reactions proposed by Kathrotia *et al.* [46] in order to be able to use the same approach for determining ignition delay periods. Ignition delay time calculations were carried out using the Chemkin II package [47] based on the 0-dimensional homogeneous reactor model with the initial composition of the mixture (see Table 1), initial temperature, and pressure behind reflected shock wave, and the pressure profile as input parameters. On the other hand, laminar flame speeds calculations based on a freely propagating flame and incorporating multi-component and thermo diffusion models were carried out using Cantera software [48].

Table 2: Details of chemical kinetic models used in this work

Reference	**Species**	**Reactions**
DLR-Mech (2021) [35]	313	2148
Mehl *et al.*[36]	317	2634
LLNL (2021)[27]	1959	10386
Cai *et al.*[16]	325	1639

3 Results and discussions

3.1 Ignition delay times

3.1.1 Comparison of experiment and modeling study

Ignition delay times of stoichiometric mixtures of OME_1, PRF90, and OME_1 / PRF90 were measured using the shock tube method at a dilution level of 1:5 with N_2, at initial pressures of about 1, 4, and 16 bar, within the temperature range of 1000 - 2000 K. Figure 3 shows the comparison of the experimental results to the results of calculations by using several detailed reaction mechanisms. Ignition delay times were measured up to 12500 µs, depending on temperature and pressure as outlined in Fig. 3. The high level of dilution applied in all the fuel-oxidizer mixtures studied reduced drastically the probability of pre-reactivity for temperatures below 1000 K; thus, measurements were made in the temperature regime between 1000-2000 K. For elevated pressures of 4 and 16 bar, post shock compression leads to shorter ignition delay times for temperatures less than 1300 K. This behavior is accounted for in modeling by providing the experimental pressure profile.

A detailed reaction model for a blend should be able to predict the experimental data for the blend as well as the individual fuels. As a result, calculations based on the DLR reaction mechanism are compared to all experimental data (blend and the individual fuels). Moreover, the experimental data for OME_1 is compared to predictions made using Cai's model. The experimental data for PRF90 are compared to model predictions using the LLNL model and the Mehl *et al.* model (see Table 2). As shown in Fig. 3(a), the measured ignition delay times for OME_1 are well reproduced by the model of Cai at 4 bar and the DLR mechanism at 16 bar. For PRF90 and the OME_1 / PRF90 blend, respectively with the results shown in Figs. 3(b) and 3(c), the DLR mechanism best matches the temperature and pressure dependence of the experimentally determined ignition delay times. However, the three models fail to match the measured data at temperatures lower than 1300 K for 1 bar, as shown in Fig. 3b. This deviation is attributed to model inadequacies because of the limited validation targets under such conditions. As a result, the findings obtained will help to improve the in-house model. Mehl's model overpredicts the measured ignition delay times of PRF90 at elevated pressures for temperatures less than 1400 K, with a maximum overprediction of 5% at around 1250 K for 16 bar. The LLNL (2021) mechanism, on the other hand, overpredicts the measured data at temperatures greater than 1450 K for all pressures, with a maximum overprediction of 60% at 2000 K for 1 bar.

The effect of addition of 70% OME_1 (by liq. vol.) to PRF90 on the ignition delay times is presented in Fig. 4 for $\varphi = 1.0$, dilution level of 1:5, and for pressures of 1, 4 and 16 bar. For completeness, the results of calculation using the DLR mechanism for a blend with 30% OME_1 (by liq. vol.) are included. The results show that ignition delay times are shortened with addition of OME_1, over the entire temperature regime. It is seen that the calculations with the DLR reaction mechanism match satisfactorily the ignition delay time data for the blend and the individual fuel components within the experimental uncertainties. The error bars on the predicted ignition delay times depict model's reaction to the experimental uncertainty error in temperature and pressure due to the error in incident shockwave. The impact of varying the OME_1 addition fraction on the ignition delay times of the mixture at 1400 K is shown in Fig. 5 for 1, 4, and 16 bar. Since it is not possible to measure ignition delay times under all these conditions, all the data points in Fig. 5 were calculated using the DLR model. The results show that increasing the volume fraction of OME_1 reduces the ignition delay times of the blend regardless of pressure, implying that OME_1 enhances the ignition of PRF90. Additionally, at all pressures, increasing the OME_1 component in the blend lowers ignition delay times in a non-linear manner.

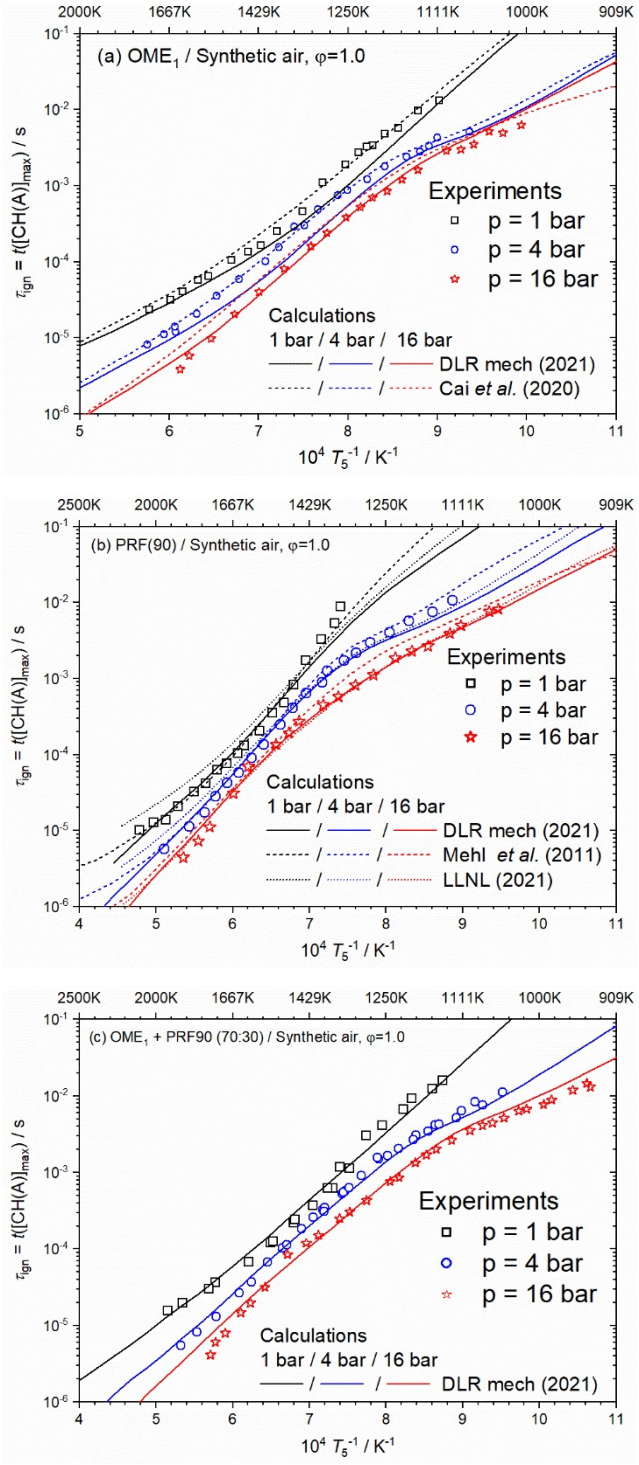

Figure 3: A comparison of measured (symbols) and calculated (lines) ignition delay times for stoichiometric mixtures of (a) OME_1 / synthetic air, (b) PRF90 / synthetic air, and (c) 70% OME_1 + 30% PRF90 / synthetic air mixtures diluted 1:5 with N_2 at initial pressures 1, 4, and 16.

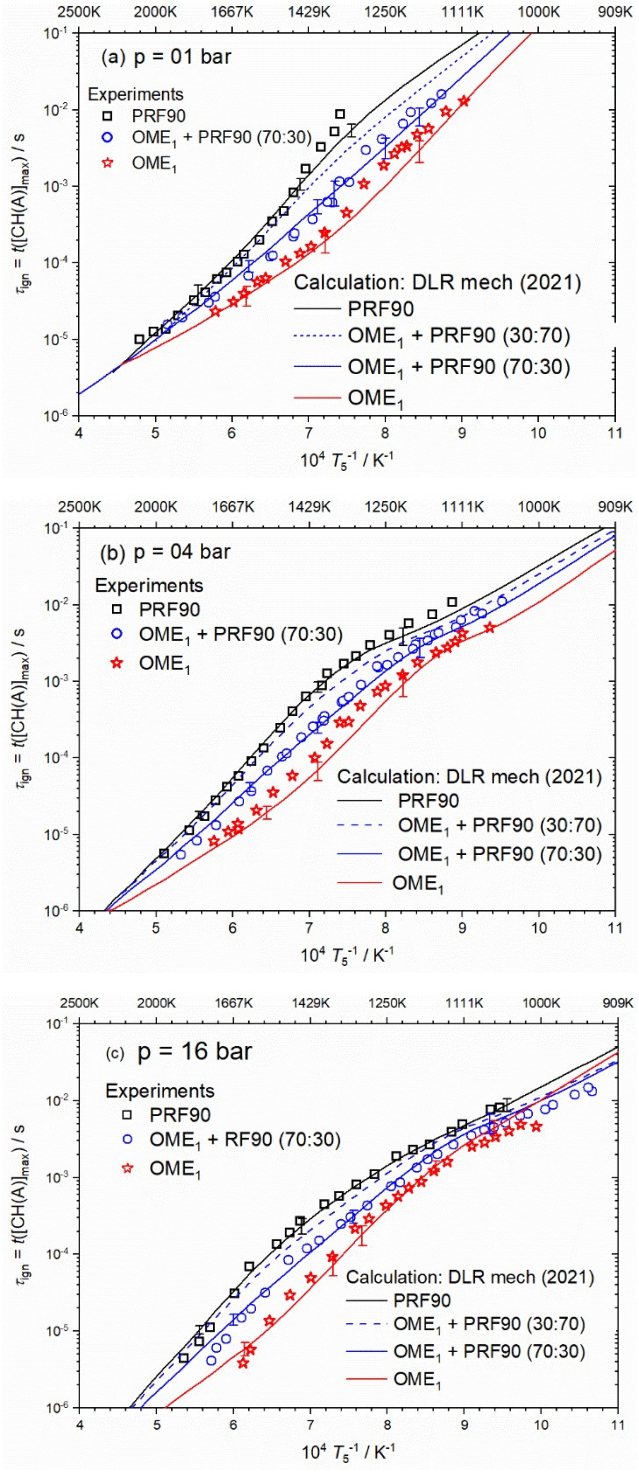

Figure 4: Measured and calculated ignition delay times of stoichiometric mixtures of OME_1 / synthetic air, PRF90 / synthetic air, and 70% OME_1 + 30% PRF90 / synthetic air mixtures diluted 1:5 with N_2 at initial pressures of (a*)* 1 bar, (b) 4 bar, and (c) 16 bar. (symbols - experiments; curves -predictions with DLR mechanism [35]).

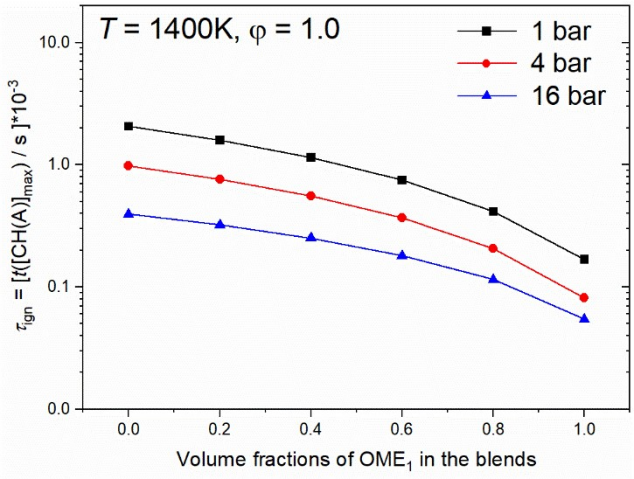

Figure 5: Ignition delay times versus addition fractions (in liq. vol.) of OME_1 in the blend at 1400 K and for φ = 1.0 at pressures of 1, 4, and 16 bar.

3.1.2 Sensitivity analysis

The sensitivity calculations for ignition delay times of stoichiometric OME_1, PRF90, and OME_1 / PRF90 (70:30) blends were conducted at φ = 1.0, dilution of 1:5 with N_2, and at a temperature of 1200 K for pressures of 1, 4, and 16 bar using the DLR mechanism. The results sorted according to p = 4 bar are presented in Fig. 6 depicting the 12 most important reactions. For all the combustible mixtures, the chain branching reaction $H+O_2 \leftrightarrow O+OH$ is the most sensitive reaction as it is the case within nearly all hydrocarbon systems. Ignition of OME_1 is also promoted by further chain propagating reactions: $CH_3+HO_2 \leftrightarrow CH_3O+OH$ and $H_2 + OH \leftrightarrow H_2O + H$. In addition, it is shown that reactions involving CH_2O (formaldehyde) which is a major intermediate in the oxidation of oxymethylene ethers are promoting the ignition process through the reactions: $CH_2O + HO_2 \leftrightarrow HCO + H_2O_2$ and $CH_2O + OH \leftrightarrow HCO + H_2O$, due to the fast decay of HCO leading to H radicals. Ignition of OME_1 is also promoted by the fuel-specific reaction $OME_1 \leftrightarrow CH_2OCH_3 + CH_3O$. The successive ß-decomposition of CH_2OCH_3 radical yields CH_2O and CH_3 radicals while CH_3O is an important species that promotes the build-up of radicals and hence accelerates ignition, for example through the reactions: $CH_3O + H \leftrightarrow CH_3 + OH$, $CH_3O + O_2 \leftrightarrow CH_2O + HO_2$, and $CH_3O + O \leftrightarrow CH_2O + OH$, besides the fast decay of CH_3O leading to H radicals. Ignition of OME_1 is mainly hindered by $CH_3 + H (+ M) \leftrightarrow CH_4 (+M)$ and $HO_2 + OH \leftrightarrow H_2O + O_2$ reactions that consume active radicals to produce stable species.

For PRF90, in addition to the chain branching reaction $H+O_2 \leftrightarrow O+OH$, ignition is promoted by the chain propagation reaction $CH_3+HO_2 \leftrightarrow CH_3O + OH$ which has the second highest sensitivity and reactions involving C_2-C_3 hydrocarbons such as C_2H_4, C_2H_3, C_3H_5, and C_3H_6. Ignition of PRF90 is mainly hindered by $HCO + M \leftrightarrow CO + H + M$ and $C_3H_5 + H (+M) \leftrightarrow C_3H_6 (+M)$ reactions. For OME_1 / PRF90 blend, ignition is promoted by the chain propagating reaction $CH_3 + HO_2 \leftrightarrow CH_3O + OH$ in addition to the chain branching reaction $H + O_2 \leftrightarrow O+OH$. Ignition of OME_1 / PRF90 blend is also promoted by fuel-specific reaction $OME_1 \leftrightarrow CH_2OCH_3 + CH_3O$ which leads to chain branching by generating CH_2OCH_3 and CH_3O radicals. This reaction accelerates the ignition process by producing

CH_2OCH_3 and CH_3O radicals, which are the major initial source of radicals as explained for OME_1. Moreover, ignition of OME_1 / PRF90 is favored by reactions of C_2H_4 and C_2H_3, respectively with O_2 and OH radicals.

According to the results of the sensitivity analysis it is observed that the relative importance of the chain propagating reaction $CH_3+HO_2 \leftrightarrow CH_3O+OH$ reaction increases with OME_1 addition. This reaction enhances the reactivity of the system by producing the more reactive OH radicals. To interpret the effect of OME_1 addition on the importance of this reaction, rate of production analysis is performed for CH_2O and HO_2 radicals and the results are presented in Fig. 7. The results reveal that CH_2O radicals are mainly formed from reactions involving CH_3O, CH_2OCH_3, and OME_1*1 radical which originate from the fuel‘s degradation. Furthermore, it is shown that CH_2O is mainly consumed via H abstraction reactions producing HCO radical which is the main source of HO_2 radical. Thus, the concentrations of CH_2O, HCO, and HO_2 are proportional to the amount of OME_1 in the blend. Due to the high concentration of HO_2 radicals in the blend, the oxidation of CH_3 radicals will be favored through the reaction $CH_3 + HO_2 = CH_3O + OH$ as opposed to other competing reactions with O and O_2. For this reason, the relative importance of this reaction increases with the increase with OME_1 blending as given in Figs. 6(a - c).

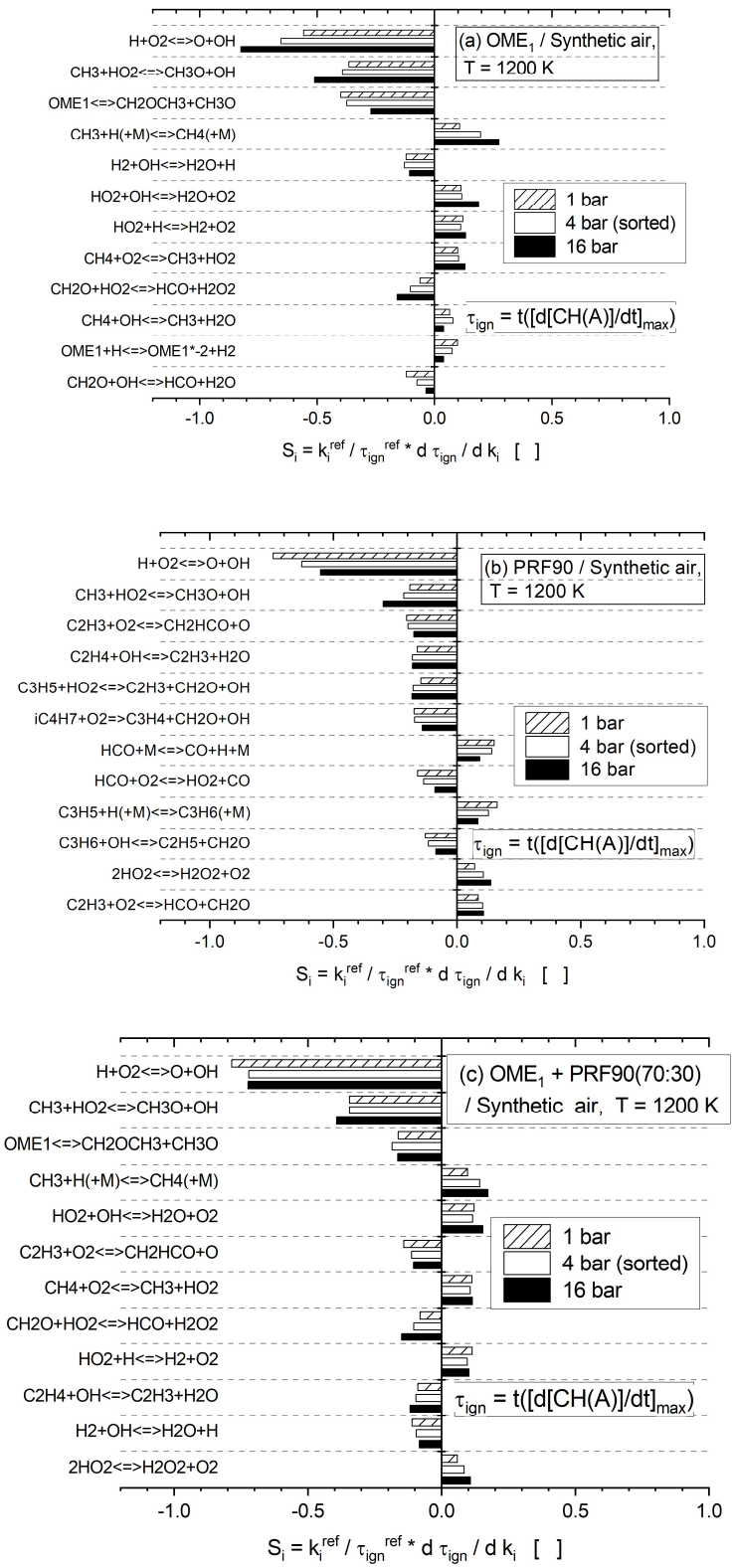

Figure 6: Normalized ignition delay time sensitivities calculated for stoichiometric mixtures of (a) OME_1 / synthetic air, (b) PRF90 / synthetic air, and (c) OME_1 + PRF90 (70:30) / synthetic air at p /bar = 1, 3 and 6, T = 1200 K, and a dilution d = 1:5 in N_2; DLR reaction model used.

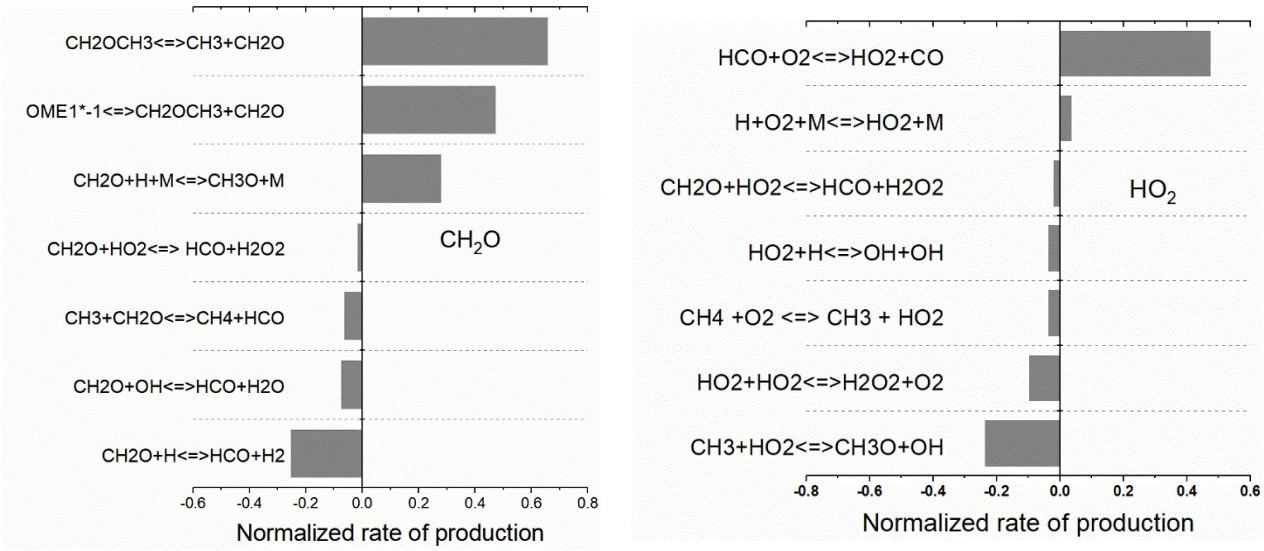

Figure 7: ROP analysis of CH_2O and HO_2 radicals during the ignition of OME_1/synthetic T = 1200 K, p = 4 bar, φ = 1.0, and a dilution d = 1:5 in N_2 calculated at 20% fuel consumption using DLR mechanism [35]. OME1*-1 represents the primary fuel radical $CH_3OCH_2OCH_2$ (COCOC*)

3.1.3 Radical mole fraction analysis

Reactions involving small radicals such as O, OH, H, HO_2, and CH_3 have a dominant role in the ignition process as demonstrated by the results of sensitivity analyses. Thus, to interpret the effect of OME_1 blending to PRF90 on ignition delay times, the mole fraction profiles of these radicals are analyzed during homogenous ignition of stoichiometric mixtures of OME_1, PRF90, and OME_1 / PRF90 (70:30) using the DLR reaction model [35]. Furthermore, HCO and CH_2O are considered, too because they are important intermediate species observed in the ignition process of oxyethylene ethers, as clearly seen from the results of the sensitivity analysis. The results are presented in Fig. 8 for equivalence ratio φ =1.0, pressure of 16 bar, temperature of 1300 K and dilution of 1:5 in N_2. These results show that the peak concentrations of O, OH, and H radicals increase sharply at about 0.2, 0.4 and 0.9 ms, respectively for OME_1, OME_1 / PRF90, and PRF90, thus signifying the onset of ignition. On the other hand, the concentrations of CH_2O, CH_3, HO_2, and HCO decrease sharply during this period, implying that they are important species for the radical pool's build-up during the pre-ignition period. It is observed that the addition of OME_1 increases the peak concentration of all radicals. An increase in the concentration of these radicals implies that the reactivity of the system increases, too; thus, ignition delay times become shorter.

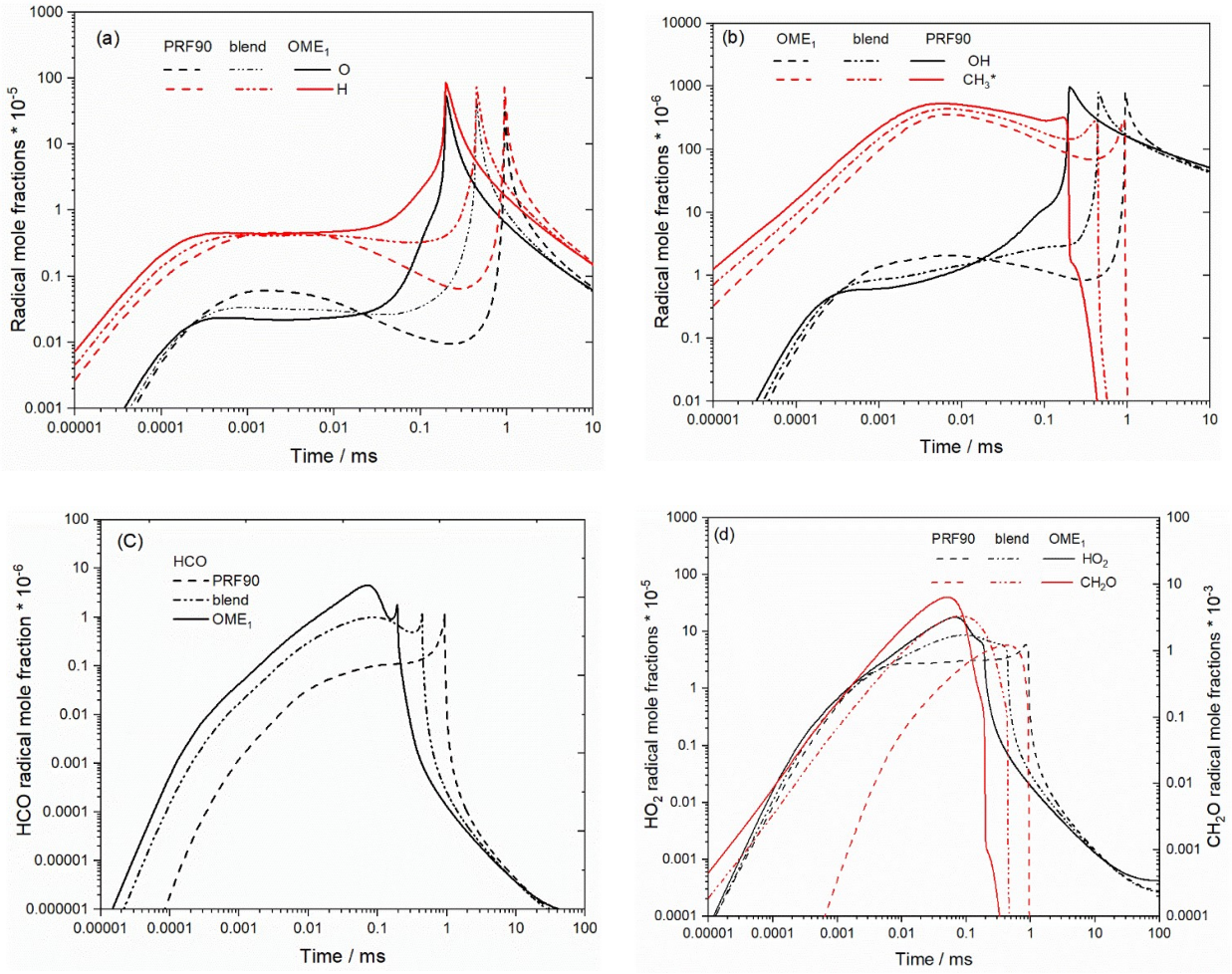

Figure 8: Mole fractions profiles of O, H (a), OH, CH_3 (b), HCO (c), and HO_2, CH_2O (d) radicals for OME_1, OME_1 / PRF90 (70:30) blend and PRF90 at φ = 1.0, T = 1300 K, p = 16 bar, and dilution d = 1:5 with N_2.

3.2 Laminar flame speeds

3.2.1 Comparison of experiments and modeling efforts

The results of the measured laminar burning velocities (LBVs) of OME_1, PRF90, and 30% OME_1 + 70% PRF90, each in mixture with air, as a function of equivalence ratio are presented in Fig. (9a) for pressures of 1, 3, and 6 bar, at an initial temperature of 473 K. Figures 9(b-d) show the comparison to the modeling results using several reaction mechanisms. The error bars included in Fig. 9 represent the maximum uncertainties observed during the measurements. The peak value of LBVs of OME_1, PRF90, and 30% OME_1 + 70% PRF90 are observed at the equivalence ratios of φ = 1.2, 1.1, and 1.1, respectively. As expected, LBVs are observed to decrease with increase in pressure. For example, the LBVs of OME_1 decrease from 103 cm/s at 1 bar to 80.4 cm/s at 3 bar and 64.8 cm/s at 6 bar. This shows that the (general) feature of LBVs decreasing with increasing pressure is reducing with pressure increasing. To the best of our knowledge, this is the first work to report LBVs of an OME_1/PRF90 blend

at both ambient and elevated pressures of 3 and 6 bar. It is seen that the LBVs of OME_1 are higher than those of the blend and PRF90 for all pressures, particularly for equivalence ratios larger than $\varphi = 0.9$. Regarding the effect of the OME_1 blending, it is seen that the addition of 30% OME_1 increases the LBVs, especially for equivalence ratios less than 1.0. At equivalence ratios larger than 1.0, the LBVs of the blend are almost in the same range particularly at 1 bar.

Calculations were performed using the DLR mechanism [35], having the capability to predict OME_1, PRF90 as well as their mixture, the mechanism from Cai *et al.*[16] for modeling OME_1, and the mechanism from Mehl *et al.*[36] for PRF90. Regarding the prediction of OME_1 shown in Fig. (9b) the DLR mechanism [35] is closer to the experimental values, with an slight underprediction of up to 5 cm/s at 1 bar and fuel rich mixtures with $1.0 \leq \varphi \leq 1.5$. For 1 bar, the same difference is found as overprediction at the fuel-lean site. When using the mechanism from Cai *et al.*[16], the maximum of the flame speed seems is shifted; hence, the deviations in terms of underprediction at the fuel-rich side and of overprediction at the fuel-lean side, respectively are larger than with the DLR mechanism. For the calculation of PRF90 (see Fig. (9d)) the mechanism of Mehl *et al.*[36] yields a nearly exact prediction of the experimental data up to $\varphi \leq 1.5$ at $p = 1$ bar. At elevated pressures, the mechanism matches the experiment up to $\varphi \leq 1.3$ (at 3 bar) and up to $\varphi \leq 1.0$ (at 6 bar), respectively. Using the DLR mechanism [35], the measured LBV data with $\varphi \leq 1.0$ are predicted exactly as well. At higher values, both mechanisms underpredict the experimental data, which is to some extent within the uncertainty range. Independent of the fuel, larger deviations may be attributed not only to the mechanisms but also to the difficult flame stabilization of fuel rich mixtures.

Values of the laminar flame speed of the mixture of PRF90 with OME_1 could only be calculated using the DLR mechanism [35]. As presented in Fig. (9c), the calculations predict the experimental LBVs data better compared to the ones of OME_1 or PRF90. The model matches the experimental values quite well, even at elevated pressures. At 1 bar, the modeling of even very fuel-rich mixtures is good, showing only a slight underprediction. This calculation also proves the result from the experiment that the addition of a significant amount of OME_1 leads only to a small increase of PRF90 being a surrogate for gasoline. Similar results were also found for the admixture of OME_4 to a diesel surrogate. In general, the decomposition and oxidation of hydrocarbons reveal a lower reactivity than OME_n explaining the lower values of the LBVs obtained for PRF90. The results from the present study as well as from a study on OME_4 / diesel surrogate [49] show that hydrocarbon components have a stronger effect on the total reaction rate of the oxidation of OME_n / fuel blends than OME_n components.

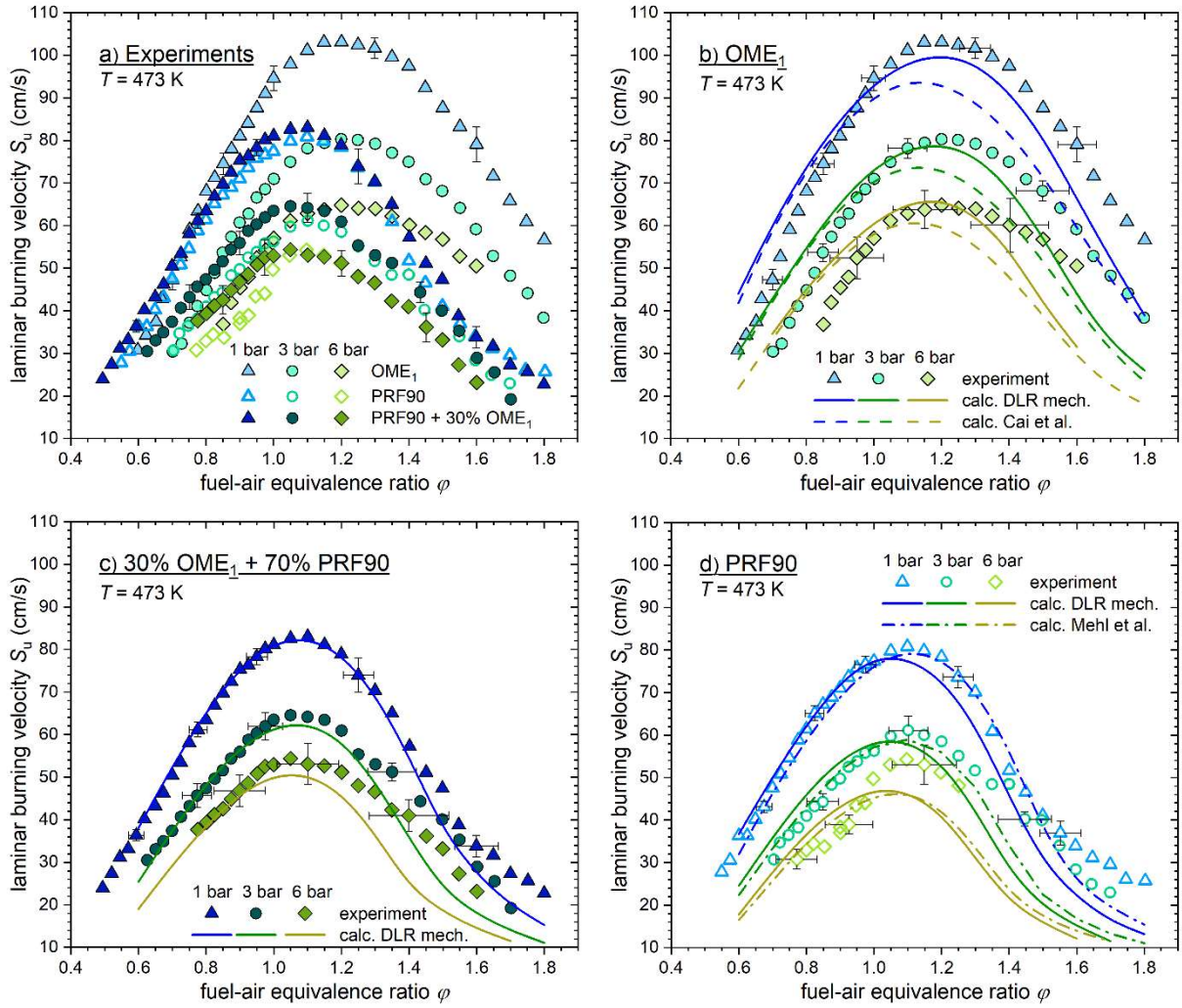

Figure 9: Results of the measured laminar burning velocities at $T = 473$ K of PRF90, neat OME_1, and 30%(w/w) OME_1 + 70%(w/w) PRF90: (a) Comparison between the experimental data and the calculated laminar flame speeds for 1 bar (b), 3 bar (c), and 6 bar (d) using mechanisms from Cai *et al.*[16] for OME_1, from Mehl *et al.*[36] for PRF90 as well as the DLR mechanism [35].

3.2.2 Sensitivity analysis

To get more information about the reaction behavior of the considered fuels regarding LBV, sensitivity analyses were performed being with the results presented in Fig. 10 and Fig. 11. First, the calculated sensitivities for the laminar flame speeds of OME_1, PRF90, and their blend of 30%(w/w) OME_1 + 70%(w/w) PRF90 at $\varphi = 1.0$, 473 K and 1 bar using the DLR reaction model [35] are shown (Fig. 10). Here, similar to the sensitivity analyses for the ignition delay times (Fig. 6), the chain branching reaction $H+O_2 \leftrightarrow O+OH$ is the most important reaction promoting the oxidation of all hydrocarbon fuels. Overall, this is the most dominant acceleration reaction for PRF90 whereas for OME_1 the chain propagation reaction via $H_2+OH \leftrightarrow H+H_2O$ also reveals a high sensitivity, even higher than other chain branching reactions, contributing to an acceleration of the flame speed data as well.

Regarding the blend of OME_1 and PRF90, the chain branching reaction via $H+O_2 \leftrightarrow O+OH$ is most dominant as well; solely the reaction of $HCO+O_2 \leftrightarrow CO+HO_2$ shows a similar sensitivity. Hence, the sensitivity analysis supports the assumption that the reaction rate of the OME_1 / PRF90 mixture is mainly controlled by the reactions of PRF90. For this fuel mixture, also the laminar flame speed sensitivities at elevated pressures were calculated (see Fig. 11) demonstrating the importance of three-body reactions. The chain termination reactions of $H+O_2(+M) \leftrightarrow HO_2(+M)$ and of $CH_3+H(+M) \leftrightarrow CH_4(+M)$, respectively decelerate the fuel's oxidation since radicals are consumed leading to a lower LBV values.

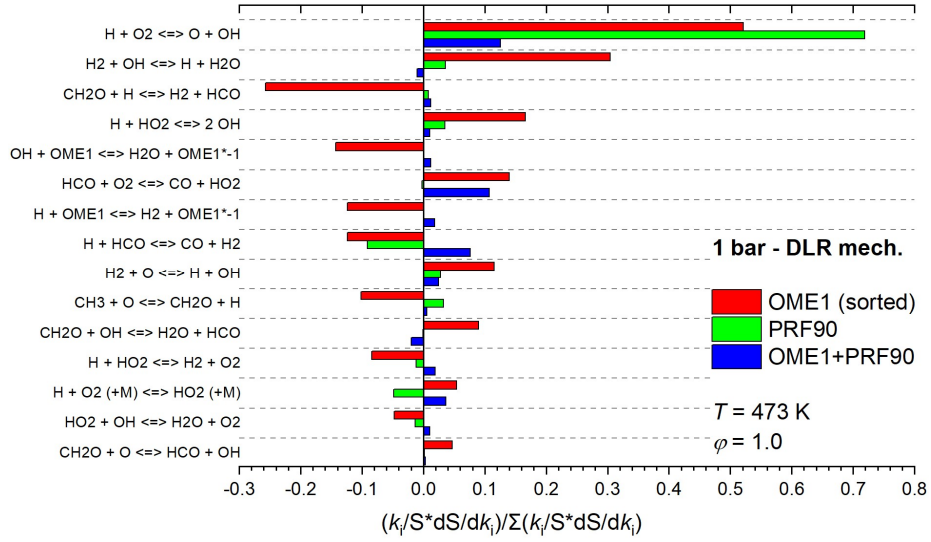

Figure 10: Laminar flame speed sensitivities calculated for stoichiometric fuel-air mixtures of OME_1, PRF90, and 30%(w/w) OME_1 + 70%(w/w) PRF90 at 473 K and 1 bar; DLR mechanism used [35].

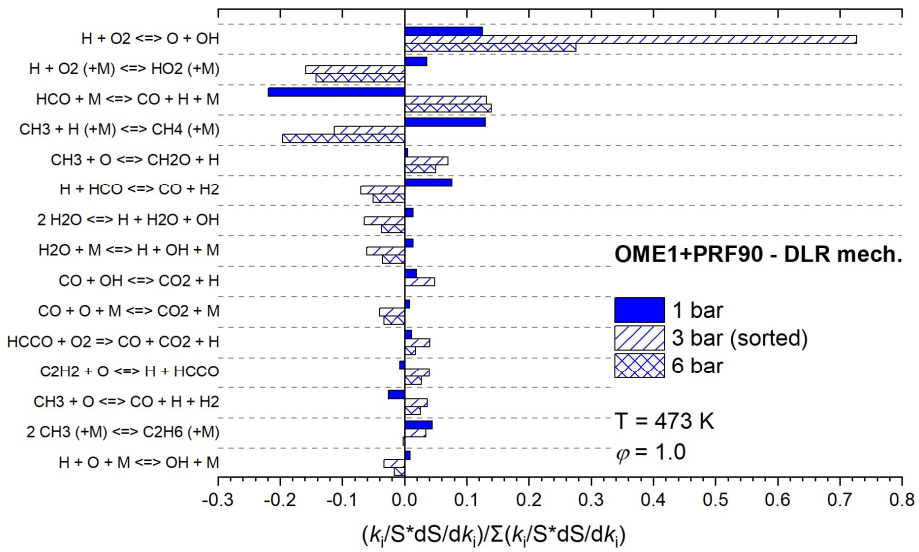

Figure 11: Laminar flame speed sensitivities calculated for a stoichiometric mixture of 30%(w/w) OME_1 + 70%(w/w) PRF90 with air at a preheat temperature T = 473 K and pressures of 1 bar, 3bar, and 6 bar; DLR mechanism [35] used.

3.2.3 Comparison to literature work

Laminar burning velocities of OME_1 have been reported in several studies in efforts to understand its flame propagation and combustion properties. In Fig. 10, a comparison is displayed for LBV measurements of OME_1 achieved from the present work (for p = 1 and 3 bar at initial temperature of T = 473 K) with literature data [50-54] for pressures of p = 1, 3 and 5 bar and covering a wide range of initial temperatures. Due to the different initial temperatures considered in the various studies, the measurements are not directly comparable. As expected, it is observed that, for constant pressure, increasing the initial temperature increases the LBV. Considering the measurements for 1 bar, the peak LBV is 46.7 cm/s at 298 K (Shrestha *et al.* [54]), 68.3 cm/s at 393 K (Eckart *et al.* [50, 51]), and 103.1 cm/s at 473 K (Ngugi *et al.* [17]) showing that the LBVs are very sensitive to an increase in the initial preheat temperature and that this effect increases with increase in temperature. Regarding the location of the peak LBV, it is seen that the location of the peak LBVs of OME_1 is at φ = 1.2 and is unaffected by variation in pressure and or initial temperature.

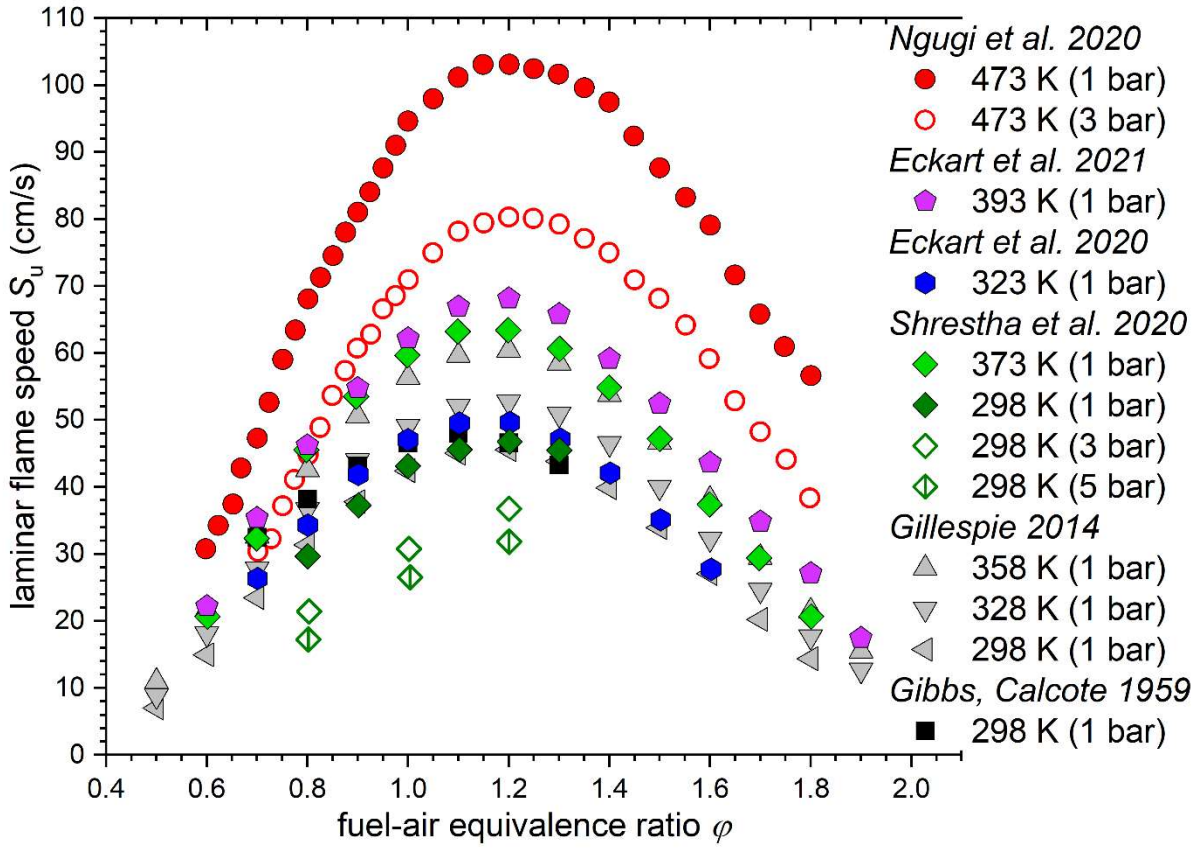

Figure 12: A comparison of laminar burning velocities of OME_1/ air: data from Ngugi *et al.* [17], Eckart *et al.*[50, 51], Shrestha *et al.* [54], Gillespie [53], and Gibbs and Calcote [52].

4 Conclusions

This work presents the results of a combined experimental and numerical study on the auto-ignition and laminar burning velocities of OME_1 / PRF90 blend. Ignition delay time measurements of OME_1, PRF90,

and OME_1 / PRF90 blend (OME_1: PRF90 = 70%: 30%, volumetric fraction) were measured behind the reflected shock waves at fuel equivalence ratio of 1.0 within the temperature range between 1000 – 2000, and at initial pressures of about 1, 4, and 16 bar. Furthermore, laminar burning velocities of OME_1, PRF90, and their blend with 30% OME_1 (w/w) were measured using a Bunsen burner and applying the cone angle method at a preheat temperature of 473 K, equivalence ratios φ between 0.6 to 1.8, and for pressures of 1, 3 and 6 bar. The experimental data were compared to the results of calculations made with the in-house DLR model (2021) for all mixtures experimentally investigated and with the public-domain models of Cai *et al. (2020)* and Mehl *et al.* (2011), respectively for OME_1 and PRF90.

In general, there was a good match between measurements and calculations with the three reaction models. Predictions with the DLR mechanism reproduced satisfactorily the experimental data for OME_1 / PRF90 blend as well as those of the individual fuel components OME_1 and PRF90. From the measurements and calculations, it is concluded that addition of OME_1 increases the reactivity of the system as depicted by the decrease in ignition delay times and the increase in laminar burning velocities. The results of the sensitivity and radical mole fraction analyses revealed that increasing OME_1 fraction in the blend increases the reactivity of the system by promoting the build-up of radicals.

This study is part of our ongoing work on the investigation of combustion properties of ethers and their admixtures with surrogate mixtures for gasoline and diesel. The results obtained in this work are enlarging the experimental data base for the improvement of the in-house model developed for describing the combustion admixtures of OME_n and surrogate mixtures for gasoline and diesel in common combustion environment. We consider this work as a step forward in understanding the combustion of blends of OMEs and PRF90.

5 Acknowledgments

We thank N. Ackermann for his help in the experimental setup. J.M. Ngũgĩ gratefully acknowledges the financial support by National Research Fund of Kenya and DAAD (Funding programme No: 57399475).

References

[1] K. Kohse-Höinghaus, Combustion in the future: The importance of chemistry, Proc. Combust. Inst. 38 (2021) 1-56.

[2] H. Fujishima, Y. Satake, N. Okada, S. Kawashima, K. Matsumoto, H. Saito, Immunology, Effects of diesel exhaust particles on primary cultured healthy human conjunctival epithelium, Ann. Allergy Asthma 110 (2013) 39-43.

[3] C.J. Smith, P.M. Forster, M. Allen, J. Fuglestvedt, R.J. Millar, J. Rogelj, K. Zickfeld, Current fossil fuel infrastructure does not yet commit us to 1.5° C warming, Nature communications 10 (2019) 1-10.

[4] D. Kodjak, Policies to reduce fuel consumption, air pollution, and carbon emissions from vehicles in G20 nations, The International Council on Clean Transportation, https://theicct.org/sites/default/files/publications/ICCT_G20-briefing-paper_Jun2015_updated.pdf, 2015.

[5] ICCT, Comments and technical recommendations on future Euro 7/VII emission standards, https://theicct.org/sites/default/files/eu-commission-euro-7-and-VI-may2021.pdf, 2021.

[6] T. Haasz, J.J. Vilchez, R. Kunze, P. Deane, D. Fraboulet, U. Fahl, E. Mulholland, Perspectives on decarbonizing the transport sector in the EU-28, Energy strateg. rev. 20 (2018) 124-132.

[7] G. Emberger, Low carbon transport strategy in Europe: A critical review, Int. J. Sustain. Transp. 11 (2017) 31-35.

[8] J. Zawieska, J. Pieriegud, Smart city as a tool for sustainable mobility and transport decarbonisation, Transp. Policy 63 (2018) 39-50.

[9] S. Deutz, D. Bongartz, B. Heuser, A. Kätelhön, L.S. Langenhorst, A. Omari, M. Walters, J. Klankermayer, W. Leitner, A. Mitsos, Cleaner production of cleaner fuels: wind-to-wheel–environmental assessment of CO_2-based oxymethylene ether as a drop-in fuel, Energy Environ. Sci. 11 (2018) 331-343.

[10] S.E. Iannuzzi, C. Barro, K. Boulouchos, J. Burger, Combustion behavior and soot formation/oxidation of oxygenated fuels in a cylindrical constant volume chamber, Fuel 167 (2016) 49-59.

[11] L. Cai, F. vom Lehn, H. Pitsch, Higher alcohol and ether biofuels for compression-ignition engine application: a review with emphasis on combustion kinetics, Energy Fuels 35 (2021) 1890-1917.

[12] H. Liu, Z. Wang, Y. Li, Y. Zheng, T. He, J. Wang, Recent progress in the application in compression ignition engines and the synthesis technologies of polyoxymethylene dimethyl ethers, Appl. Energy 233 (2019) 599-611.

[13] A. Omari, B. Heuser, S. Pischinger, Potential of oxymethylenether-diesel blends for ultra-low emission engines, Fuel 209 (2017) 232-237.

[14] A. Omari, B. Heuser, S. Pischinger, C. Rüdinger, Potential of long-chain oxymethylene ether and oxymethylene ether-diesel blends for ultra-low emission engines, Appl. Energy 239 (2019) 1242-1249.

[15] J. Liu, H. Wang, Y. Li, Z. Zheng, Z. Xue, H. Shang, M. Yao, Effects of diesel/PODE (polyoxymethylene dimethyl ethers) blends on combustion and emission characteristics in a heavy duty diesel engine, Fuel 177 (2016) 206-216.

[16] L. Cai, S. Jacobs, R. Langer, F. vom Lehn, K.A. Heufer, H. Pitsch, Auto-ignition of oxymethylene ethers (OME_n, n=2–4) as promising synthetic e-fuels from renewable electricity: shock tube experiments and automatic mechanism generation, Fuel 264 (2020) 116711.

[17] J.M. Ngugi, S. Richter, M. Braun-Unkhoff, C. Naumann, U. Riedel, An investigation of fundamental combustion properties of the oxygenated fuels DME and OME_1, Proc. ASME Turbo Expo. 2020, 2020.

[18] J. Herzler, M. Fikri, C. Schulz, High-pressure shock-tube study of the ignition and product formation of fuel-rich dimethoxymethane (DMM)/air and CH_4/DMM/air mixtures, Combust. Flame 216 (2020) 293-299.

[19] A. Nicolle, N. Naser, T. Javed, N. Rankovic, S.M. Sarathy, Autoignition characteristics of ethers blended with low cetane distillates, Energy Fuels 33 (2019) 6775-6787.

[20] G. Kalghatgi, H. Levinsky, M. Colket, Future transportation fuels, Prog. Energy Combust. Sci. 69 (2018) 103-105.

[21] J. Badra, Y. Viollet, A. Elwardany, H.G. Im, J. Chang, Physical and chemical effects of low octane gasoline fuels on compression ignition combustion, Appl. Energy 183 (2016) 1197-1208.

[22] Z. Gao, E. Hu, Z. Xu, G. Yin, Z. Huang, Low to intermediate temperature oxidation studies of dimethoxymethane/n-heptane blends in a jet-stirred reactor, Combust. Flame 207 (2019) 20-35.

[23] D. Goeb, M. Davidovic, L. Cai, P. Pancharia, M. Bode, S. Jacobs, J. Beeckmann, W. Willems, K.A. Heufer, H. Pitsch, Oxymethylene ether–n-dodecane blend spray combustion: Experimental study and large-eddy simulations, Proc. Combust. Inst. 38 (2021) 3417-3425.

[24] E. Hu, Z. Gao, Y. Liu, G. Yin, Z. Huang, Experimental and modeling study on ignition delay times of dimethoxy methane/n-heptane blends, Fuel 189 (2017) 350-357.

[25] S. Ren, Z. Wang, B. Li, H. Liu, J. Wang, Development of a reduced polyoxymethylene dimethyl ethers ($PODE_n$) mechanism for engine applications, Fuel 238 (2019) 208-224.

[26] Q. Lin, K.L. Tay, D. Zhou, W. Yang, Development of a compact and robust Polyoxymethylene Dimethyl Ether 3 reaction mechanism for internal combustion engines, Energy Convers. Manag. 185 (2019) 35-43.

[27] S. Cheng, C. Saggese, D. Kang, S.S. Goldsborough, S.W. Wagnon, G. Kukkadapu, K. Zhang, M. Mehl, W.J. Pitz, Autoignition and preliminary heat release of gasoline surrogates and their blends with ethanol at engine-relevant conditions: Experiments and comprehensive kinetic modeling, Combust. Flam.228 (2021) 57-77.

[28] D. Kang, A. Fridlyand, S.S. Goldsborough, S.W. Wagnon, M. Mehl, W.J. Pitz, M.J. McNenly, Auto-ignition study of FACE gasoline and its surrogates at advanced IC engine conditions, Proc. Combust. Inst. 37 (2019) 4699-4707.

[29] Y. Ra, R.D. Reitz, A reduced chemical kinetic model for IC engine combustion simulations with primary reference fuels, Combust. Flam. 155 (2008) 713-738.

[30] H. Selim, S.Y. Mohamed, N. Hansen, S.M. Sarathy, Premixed flame chemistry of a gasoline primary reference fuel surrogate, Combust. Flame 179 (2017) 300-311.

[31] J.C. Andrae, Development of a detailed kinetic model for gasoline surrogate fuels, Fuel 87 (2008) 2013-2022.

[32] J.C. Andrae, P. Björnbom, R. Cracknell, G. Kalghatgi, Autoignition of toluene reference fuels at high pressures modeled with detailed chemical kinetics, Combust. Flam.149 (2007) 2-24.

[33] K. Fieweger, R. Blumenthal, G. Adomeit, Self-ignition of SI engine model fuels: a shock tube investigation at high pressure, Combust. Flame 109 (1997) 599-619.

[34] S. Richter, M. Braun-Unkhoff, J. Herzler, T. Methling, C. Naumann, U. Riedel, An investigation of combustion properties of a gasoline primary reference fuel surrogate blended with butanol, Proc. ASME Turbo Expo. 2019, GT2019-90911.

[35] T. Kathrotia, P. Oßwald, C. Naumann, S. Richter, M. Köhler, Combustion kinetics of alternative jet fuels, Part-II: Reaction model for fuel surrogate, Fuel 302 (2021) 120736.

[36] M. Mehl, W.J. Pitz, C.K. Westbrook, H.J. Curran, Kinetic modeling of gasoline surrogate components and mixtures under engine conditions, Proc. Comb. Inst., 2011, 193-200.

[37] J. Herzler, J. Herbst, T. Kick, C. Naumann, M. Braun-Unkhoff, U. Riedel, Alternative fuels based on biomass: An investigation of combustion properties of product gases, J. Eng. Gas Turbines 135 (2013).

[38] T. Methling, S. Richter, T. Kathrotia, M. Braun-Unkhoff, C. Naumann, U. Riedel, An investigation of combustion properties of butanol and its potential for power generation, J. Eng. Gas Turbines Power 140 (2018).

[39] J. Herzler, C. Naumann, Shock tube study of the ignition of lean CO/H_2 fuel blends at intermediate temperatures and high pressure, Combust. sci. technol. 180 (2008) 2015-2028.

[40] M. Braun-Unkhoff, J. Dembowski, J. Herzler, J. Karle, C. Naumann, U. Riedel, Alternative fuels based on biomass: An experimental and modeling study of ethanol cofiring to natural gas, J. Eng. Gas Turbines Power 137 (2015).

[41] C. Naumann, C. Janzer, U. Riedel, Ethane/nitrous oxide mixtures as a green propellant to substitute hydrazine: validation of reaction mechanism, Proc. European Combust. Meeting Lisbon, Portugal, 2019, 14-17.

[42] P. Roth, Vergleichende Messungen der Schwingungsenergie-Anregung von CO hinter Stosswellen und der Schwingungsenergie-Abregung in Expansionswellen, Institut für Reaktionskinetik, Deutsche Forschungs- und Versuchsanstalt für Luft- und Raumfahrt e.V. (DFVLR), 1971.

[43] E.L. Petersen, A shock tube and diagnostics for chemistry measurements at elevated pressures with application to methane ignition, Stanford University (USA), 1999.

[44] E.L. Petersen, Interpreting endwall and sidewall measurements in shock-tube ignition studies, Combust. Sci. Technol. 181 (2009) 1123-1144.

[45] S. Richter, T. Kathrotia, C. Naumann, T. Kick, N. Slavinskaya, M. Braun-Unkhoff, U. Riedel, Experimental and modeling study of farnesane, Fuel 215 (2018) 22-29.

[46] T. Kathrotia, U. Riedel, A. Seipel, K. Moshammer, A. Brockhinke, Experimental and numerical study of chemiluminescent species in low-pressure flames, Appl. Phys. B 107 (2012) 571-584.

[47] A.E. Lutz, R.J. Kee, J.A. Miller, SENKIN: A FORTRAN program for predicting homogeneous gas phase chemical kinetics with sensitivity analysis, Sandia National Labs., Livermore, CA (USA), 1988.

[48] D.G. Goodwin, R.L. Speth, H.K. Moffat, B.W. Weber, Cantera: An Object-oriented Software Toolkit for Chemical Kinetics, Thermodynamics, and Transport Processes. https://www.cantera.org, doi:10.5281/zenodo.4527812. doi: 10.5281/zenodo.4527812.

[49] S. Richter, T. Kathrotia, M. Braun-Unkhoff, C. Naumann, M. Köhler, Influence of oxymethylene ethers (OME_n) in mixtures with a diesel surrogate, Energies 14 (2021) 7848.

[50] S. Eckart, L. Cai, C. Fritsche, F. vom Lehn, H. Pitsch, H. Krause, Laminar burning velocities, CO, and NO_x emissions of premixed poly(oxymethylene) dimethyl ether flames, Fuel 293 (2021) 120321.

[51] S. Eckart, C. Fritsche, C. Krasselt, H. Krause, Determining the laminar burning velocity of nitrogen diluted dimethoxymethane (OME_1) using the heat-flux burner method: Numerical and experimental investigations, Int. J. Energy Research 45 (2020) 2824-2836.

[52] G.J. Gibbs, H.F. Calcote, Effect of molecular structure on burning velocity, J. Chem. Eng. data 4 (1959) 226-237.

[53] F.R. Gillespie, An experimental and modelling study of the combustion of oxygenated hydrocarbons, School of Chemistry, National University of Ireland–Galway, 2014.

[54] K.P. Shrestha, S. Eckart, A.M. Elbaz, B.R. Giri, C. Fritsche, L. Seidel, W.L. Roberts, H. Krause, F. Mauss, A comprehensive kinetic model for dimethyl ether and dimethoxymethane oxidation and NO_x interaction utilizing experimental laminar flame speed measurements at elevated pressure and temperature, Combust. Flame 218 (2020) 57-74.